

Performance prediction and optimization of an organic Rankine cycle (ORC) for waste heat recovery using back propagation neural network

Yong-qiang Feng^a, Yu-Zhuang Liu^a, Xin Wang^a, Zhi-Xia He^{b,*}, Tzu-Chen Hung^{c,*}, Qian Wang^a, Huan Xi^{d,e}

^a School of Energy and Power Engineering, Jiangsu University, Zhenjiang, China

^b Institute for Energy Research, Jiangsu University, Zhenjiang, China

^c Department of Mechanical Engineering, National Taipei University of Technology, Taipei, Taiwan

^d Key Laboratory of Thermo-Fluid Science and Engineering of Ministry of Education, School of Energy and Power Engineering, Xi'an Jiaotong University, Xi'an 710049, China

^e New Energy (Photovoltaic) Industry Research Center, Qinghai University, Xining 810016, China



ARTICLE INFO

Keywords:

BP neural network

BP-ORC model

Organic Rankine Cycle (ORC)

Multi-objective optimization

ABSTRACT

Performance prediction and multi-objective optimization for an organic Rankine cycle (ORC) using back propagation (BP) neural network are investigated in this study. A 3 kW ORC experiment platform is used to obtain 950 sets of basic experimental data, and a BP-ORC model using back propagation neural network is established by training the experimental data. The prediction accuracy of the BP-ORC model is analyzed according to the errors of the training samples and test samples. The effects of six operation parameters on thermal efficiency and net output work are addressed. The Pareto optimal frontier for maximum net output work and maximum thermal efficiency is examined. The results demonstrate that the prediction error of BP-ORC model is very low, and the system performance can be improved by adjusting several operating parameters experimentally according to the model prediction. A tradeoff relation is appeared between net output work and thermal efficiency. The optimal thermal efficiency and net output work for Pareto-optimal solution are obtained.

1. Introduction

Thermal energy is one of the most conventional energy utilization forms in human society. About 85–90% of energy can be converted into thermal energy for utilization. However, the utilization rate is low, and many heat resources are not fully used due to the limitation of the technology level. These waste heat resources are roughly divided into high, medium, and low-temperature waste heat [1]. Organic Rankine cycle (ORC) is an effective method to utilize the medium and low-temperature waste heat resources [2].

Numerous researches were conducted to improve the ORC system overall efficiency from the theoretical analysis. Tian et al. [3–5] examined a working fluid selection for basic ORC and two-stage ORC to recover the waste heat from internal combustion engine exhaust. Similar study was conducted by Song et al. [6], and they stated that the net output work can reach a maximum of 115.1 kW. Shu et al. [7] compared the ORC system with different configuration from the viewpoint of economic performance. Dong et al. [8] adopted the radial turbine as the

expander in the ORC and found that the high-pressure ratio and mass flow rate would reduce turbine efficiency. Wang et al. [9] used the low-pressure saturated steam as the heat source for ORC, reporting that component parameters should be considered in the optimization process. Uusitalo et al. [10] coupled the evaporator of ORC with the engine and conducted a parametric analysis using different working fluids. Javanshir et al. [11] used different working fluids to compare the cycling performance of supercritical ORC and subcritical ORC systems and proposed the novel expression of the thermal efficiency for these two types of ORC.

In order to accelerate the industrialization process of ORC, a number of studies focused on the ORC experimental test. Jang et al. [12] evaluated the ORC system by changing external parameters and internal factors, revealing that external parameters greatly affected the system performance and the expander pressure difference greatly affected its mechanical efficiency. Lin et al. [13] examined the basic operation characteristics on a 10 kW ORC system, stating that the pressure ratio and superheat had a significant influence on the system performance. The maximum measured power and net thermal efficiency were 6.2 kW

* Corresponding authors.

E-mail addresses: zxhe@ujs.edu.cn (Z.-X. He), tchung@ntut.edu.tw (T.-C. Hung).

| Nomenclature | | Acronyms |
|----------------------|--------------------------|--|
| h | specific enthalpy, kJ/kg | ANN artificial neural network |
| \dot{m} | mass flow rate, kg/s | ABC artificial bees' colony |
| M | torque, N m | BP back propagation |
| n | rotational speed, r/min | eva evaporator |
| net | net | exp expander |
| \dot{Q} | energy, kW | LM Levenberg-Marguardt |
| T | transpose of the matrix | MSE mean square error |
| <i>Greek symbols</i> | | NSGA-II Nondominated sorting genetic algorithm-II |
| η | efficiency | ORC organic Rankine cycle |
| <i>Subscripts</i> | | pump pump |
| in | inlet | R correlation coefficient |
| out | outlet | TOPSIS Technique for Order Preference by Similarity to Ideal Situation |

and 8.9%, respectively. Liu et al. [14] conducted the ORC steady-state and dynamic performance tests, reporting that load reduction could not play a role in stabilizing the system. Sun et al. [15] considered the pressure loss of each device in ORC, and they found that the result of pressure losses in a reduction in net output work of 16.1% and thermal efficiency of 17.0%, accordingly. In addition, many researchers paid attention to the experimental comparison between pure and mixture working fluids[16]. In the experiments, the maximum net output work was 7.68 kW and thermal efficiency was 6.15%. Similar research was conducted by Feng et al. [17], and they found that 0.67R245fa/0.33R123 obtained a relatively higher thermal efficiency than the pure working fluids. Feng et al. [18,19] conducted a detailed analysis on the four main components using 3 kW and 10 kW ORC test benches under different operating conditions. Wang et al. [20] and Liu et al. [21] studied the off-design working conditions of ORC. Wang et al. [20] analyzed the fluctuation range of the experimental data, concluding that the maximum pressure and temperature fluctuations are found at the pump outlet and the evaporator outlet. Liu et al. [21] studied the effect of working fluids charge on system's parameters. Results showed that overcharging working fluids would increase the expander output power, while undercharging working fluids would cause cavitation of the pump.

Numerous ORC experimental test were conducted, however how to predict the unknown or unmeasured data and obtain the optimal operation parameters are still well reported. Machine learning methods have been receiving increasing attention in ORC. The artificial neural network (ANN) technology was widely used to establish predictive models because of its self-learning, nonlinearity, and arbitrary function approximation ability. Yang et al. [22] conducted the ORC performance prediction and optimization for diesel engines, and the optimal performance parameters and operation parameters were yielded. Arslan et al. [23] applied an optimization for supercritical ORC-Binary system using ANN, stating that Levenberg-Marguardt (LM) was the best algorithm applied to this system. Luo et al. [24] studied a prediction method of sub-critical ORC characteristics based on ANN, which can quickly predict the performance of systems using different working fluids. Palagi et al. [25] used ANN to derive an alternative model for ORC multi-objective optimization, and reported that the alternative model was more suitable for dealing with optimization problems with non-linear constraints. Emadi et al. [26] applied genetic algorithms and ANN on multi-objective optimization for a new multi-generation system. ANN was mainly used to reduce modeling time and save calculation costs. Rashidi et al. [27] proposed a novel method combining ANN and artificial bees' colony (ABC) for optimizing the regenerative Rankine cycle. Ziviani et al. [28] established an ANN model for an open scroll expander in ORC. Compared with existing semi-empirical models for scroll expanders, this ANN model has higher accuracy.

Based on the brief discussion above, many researches applied ANN technique. However, most of them only regarded ANN technology as a means of auxiliary optimization and neglected the essence of ANN, which is a method to provide a prediction based on existing data. Our group conducted more experimental test on a 3 kW ORC experimental prototype [29–32]. Using ANN to predict the unknown or unmeasured experimental data may be a good way to save the experimental consumption. And therefore, to obtain the optimum system performance and operation parameters, based on 950 sets ORC experimental data, a BP-ORC model is established and validated. The parametric analysis is addressed, while a further bi-objective optimization for maximum net output work and maximum thermal efficiency is examined.

2. Experimental setup description

2.1. ORC test bench description

Fig. 1 shows a schematic diagram of a 3 kW ORC experimental prototype, and Fig. 2 represents the laboratory test bench. R245fa is adopted as the working fluids, and its thermal properties are displayed in Table 1. The system consists of three parts: heat source loop, ORC loop, and cooling water loop.

2.1.1. Heat source loop

The heat source part in this work is mainly due to circulation of conducting oil. The black tank is shown in Fig. 2 which is a conducting oil boiler heated by electricity. The heat source temperature can be controlled by adjusting the power input. The heated conducting oil is exchanged with the liquid R245fa in the evaporator. An axial pump powers the circulation of conducting oil.

2.1.2. ORC loop

The ORC waste heat conversion part mainly includes an evaporator, an expander, a working pump, and a condenser. The plate heat exchangers are selected as evaporator and condenser, a scroll expander and a plunger pump are adopted. The basic parameters are listed in Tables 2–4. In short, the ORC is a cycle of endothermic-work-cooling-pressure. The scroll expander is linked with a generator through a belt so that the expander drives the generator to generate electricity. The electricity produced by the generator is consumed by the resistance-capacitance, as shown in Fig. 1(b).

2.1.3. Cooling water loop

The cooling water is used to cooldown through removing the heat from the condenser. Heat is transferred to the environment in cooling towers, which are installed outdoors. There is also a pump to power the

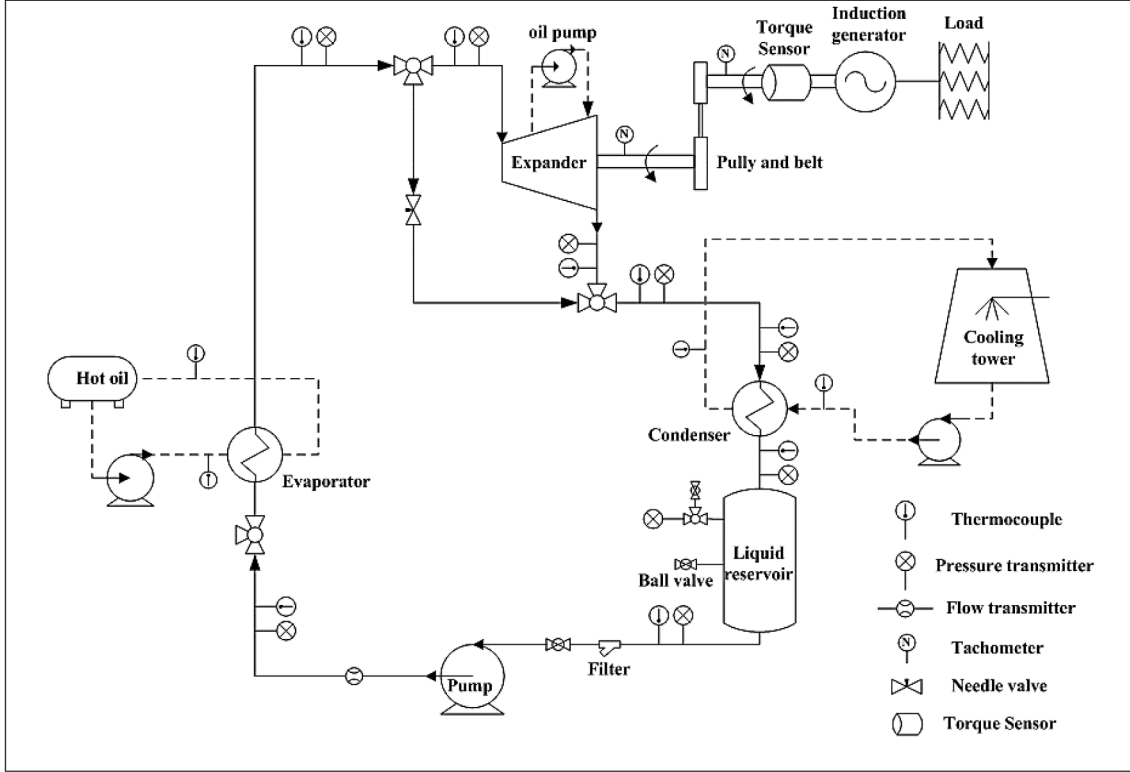


Fig. 1. The schematic diagram of a 3 kW ORC waste heat generation system.

circulation of cooling water.

2.2. Measurement devices and operation method

This experimental measurement mainly includes pressure, temperature, and flow rate. Diaphragm pressure transmitters are used for pressure measurement, T-type thermocouples are used for temperature measurement, and a vortex flowmeter is adopted for flow measurement. The flowmeter is placed at the working pump outlet to measure the volume flow rate of R245fa. The flow rate is adjusted by adjusting the working pump frequency, while the heat source temperature is adjusted by changing the heat input. The working fluid mass flow rate is raised stepwise by pump frequency, while the heat source temperature is adjusted by changing the mass flow rates of conduction oil. The experimental data is firstly recorded when the heat source temperatures are within a lower fluctuation ranging from -0.5 to 0.5 K. After 20 min steady operation, the record is terminated. In this study, 950 test points are selected for training and testing the BP-ORC model. The parameters of these test points are shown in Table 5.

The net output work and thermal efficiency are two important evaluation indexes for the ORC system. The definition of net output work (\dot{W}_{net}) is the difference between the expander shaft work (\dot{W}_{exp}) and pump shaft work ($\dot{W}_{\text{sh,pump}}$). The thermal efficiency (η_{th}) is the ratio between the net output work and evaporator heat transfer rate (\dot{Q}_{eva}).

The equations for system thermal efficiency and net output work are represented as follows.

$$\dot{W}_{\text{net}} = \dot{W}_{\text{sh,exp}} - \dot{W}_{\text{sh,pump}} \quad (1)$$

$$\eta_{\text{th}} = \frac{\dot{W}_{\text{net}}}{\dot{Q}_{\text{eva}}} \quad (2)$$

$$\dot{Q}_{\text{eva}} = \dot{m}(h_{\text{eva,in}} - h_{\text{eva,out}}) \quad (3)$$

$$\dot{W}_{\text{sh,exp}} = \frac{2\pi}{60} M_{\text{exp}} n_{\text{exp}} \quad (4)$$

$$\dot{W}_{\text{sh,pump}} = \dot{m}(h_{\text{in,pum}} - h_{\text{out,pump}}) \quad (5)$$

where M_{exp} and n_{exp} are expressed the torque and rotational speed, respectively.

3. Model and evaluation index of BP neural network

3.1. BP neural network

BP neural network is a kind of ANN, which is divided into an input layer, hidden layer, and output layer. It is a kind of multi-layer forward neural network. Its biggest characteristic is the reverse transmission of signals and errors. The initial weights are randomly set and then modified according to the differences between the training data (the calculated values in the training process) and the output data (the real values that the trainings want to achieve) in the back propagation. Forward and backward processes are repeated until the differences between the training data and output data meet the training precision (the max value that is acceptable for the mean error between training data and real data) [33]. The standard BP neural network uses a gradient descent algorithm, and the network weights are adjusted inversely along the gradient of the performance function. Therefore, the predicted value keeps getting closer to the real value.

To connect input database from Layer $n-1$, and output data to Layer $n+1$, the equation for a single neuron in Layer n can be expressed as:

$$x_j^n = f \left(\sum_{i=1}^n x_i^{n-1} w_i^n + b^n \right) \quad (6)$$

where x_j^n is the output data of node j in layer n ; i is the number of input node (or signal) from previous layer. x_i^{n-1} is the input data from node i in previous layer $n-1$; w_i^n is the weights of input data x_i^{n-1} ; b^n is the

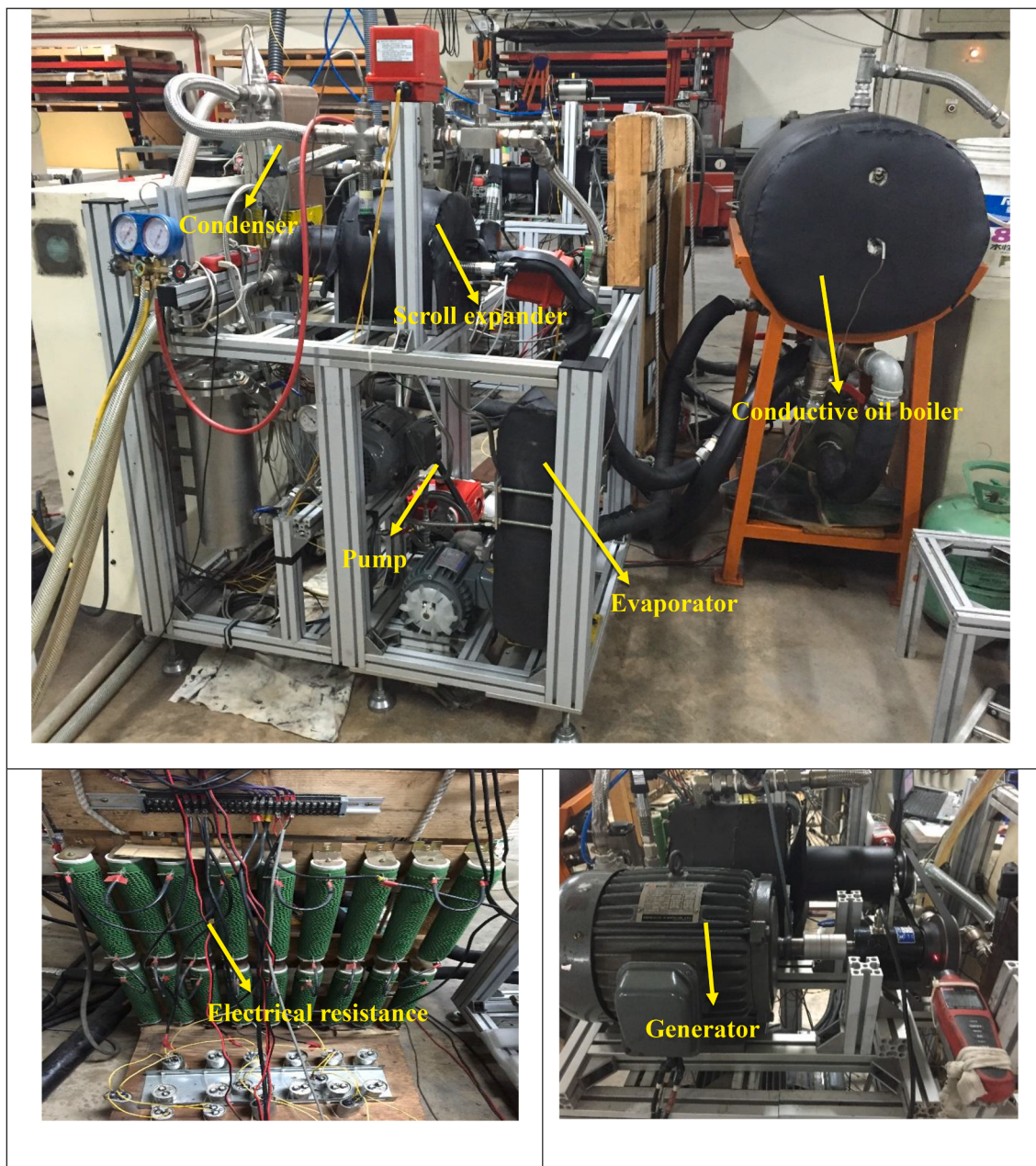


Fig. 2. The laboratory test system.

Table 1
Basic thermodynamic and environmental properties of R245fa.

| Parameter | Value | Unit |
|----------------------|--------|------|
| Working fluid | R245fa | |
| Boiling point | 15.14 | °C |
| Critical temperature | 154 | °C |
| Critical pressure | 36.51 | bar |
| ODP | 0 | |
| GWP | 950 | |

bias of the node; $f(x)$ is the transfer function of this neuron, which is usually set as sigmoid function:

$$f(x) = \text{Tansig}(x) = \frac{e^x - e^{-x}}{e^x + e^{-x}}, f(x) \in (0, 1) \quad (7)$$

The output function can be expressed as:

Table 2
Basic parameters of heat exchangers.

| Parameter | Value | Unit |
|-----------------------------|-------|----------------|
| Maximum working temperature | 200 | °C |
| Maximum working pressure | 30 | bar |
| Total volume | 8.848 | L |
| Heat transfer area | 4.175 | m ² |

Table 3
Basic parameters of the expander.

| Parameter | Value | Unit |
|--------------------|-------|--------------------|
| Volume ratio | 2.95 | |
| Base circle radius | 3.485 | mm |
| Tooth height | 32.2 | mm |
| Inspiratory volume | 18.43 | m ³ /hr |

Table 4
Basic parameters of the pump.

| Parameter | Value | Unit |
|--------------------------|--------------|------|
| Type | Plunger pump | |
| Maximum working pressure | 20 | bar |
| Temperature resistance | 40 | °C |
| Maximum flow rate | 12 | LPM |

Table 5
The parameters of test points.

| Test points | P _{pout} (bar) | T _{exp, out} (°C) | P _{exp, out} (bar) | T _{exp, in} (°C) | P _{exp, in} (bar) | M (kg/s) | η | W _{net} (kW) |
|-------------|----------------------------|-------------------------------|--------------------------------|------------------------------|-------------------------------|-------------|-------|--------------------------|
| 1 | 7.51 | 60.2 | 2.01 | 79.8 | 7.04 | 0.157 | 4.67% | 0.98 |
| 2 | 7.44 | 60.2 | 2.00 | 80.5 | 7.03 | 0.163 | 5.05% | 1.15 |
| 3 | 7.51 | 60.0 | 2.00 | 79.6 | 7.03 | 0.175 | 4.65% | 1.07 |
| | | | | | | | | |
| 948 | 6.24 | 64.3 | 1.89 | 79.8 | 5.93 | 0.172 | 3.95% | 0.83 |
| 949 | 6.20 | 64.1 | 1.88 | 79.3 | 5.88 | 0.126 | 3.81% | 0.58 |
| 950 | 6.14 | 64.1 | 1.88 | 78.8 | 5.84 | 0.205 | 3.66% | 0.84 |

$$f(x) = x, f(x) \in (-\infty, +\infty) \quad (8)$$

3.2. BP-ORC neural network model

For the inputs of BP neural network, six parameters such as pump outlet pressure, expander outlet pressure and temperature, expander inlet pressure and temperature, and mass flow rate are selected as the input layer parameters. The system thermal efficiency and net output work are applied as the output layer parameters. A single hidden layer BP-ORC model is constructed to train, predict, and optimize the 3 kW ORC experimental data. Fig. 3 shows the BP-ORC model with a single hidden layer.

3.3. Evaluation index of BP-ORC neural network model

To better evaluate the BP-ORC model, mean square error (MSE) and correlation coefficient (R) are applied as evaluation indices. Higher prediction accuracy can be represented by a smaller MSE value and a

larger R-value. The equations for MSE and R are represented by Eqs. (9) and (10), respectively.

$$MSE = \frac{1}{Q} \sum_{k=1}^Q [y(k) - t(k)]^2 \quad (9)$$

$$R = \frac{(y - \bar{y})(t - \bar{t})^T}{\sqrt{(y - \bar{y})(y - \bar{y})^T} \sqrt{(t - \bar{t})(t - \bar{t})^T}} \quad (10)$$

where $y(k)$ and $t(k)$ are the prediction value and experiment data, respectively; y and t are the mean values of prediction and experiment data, respectively.

4. Results and discussion

4.1. Parameters choose for BP-ORC model

After the BP-ORC model is established successfully, its parameters need to be set to meet the prediction requirements. The parameters mainly include learning rate, training function, and hidden layer neural number. The learning rate determines the moving amplitude of the neural network weight in the gradient direction. Generally speaking, a high learning rate may cause the training not to converge, while a low learning rate may make the training become reliable, but the optimization process will take a long time. Therefore, the determination of the learning rate is very important for training the model. Fig. 4 demonstrates the effect of different learning rates on model accuracy. R1 and R2 represent the correlation coefficients of thermal efficiency and net output work, respectively. The learning rates selected for this training ranges from 0.05 to 0.5. As can be seen from Fig. 4, the MSE and R of the model show a negative correlation trend. When the learning rate is 0.45, the minimum MSE of 0.000473 is obtained, while R1 and R2 yield the maximum value of 0.9991 and 0.9982, respectively.

The training functions of the BP-ORC neural network model are usually selected as follows: trainlm, trainrp, traingdm, traingd, and traincgb. Different training functions have their own advantages and disadvantages. Fig. 5 shows the effect of the above five training functions on model accuracy. It can be seen that the model prediction accuracy is the best when trainlm is adopted as the training function. The

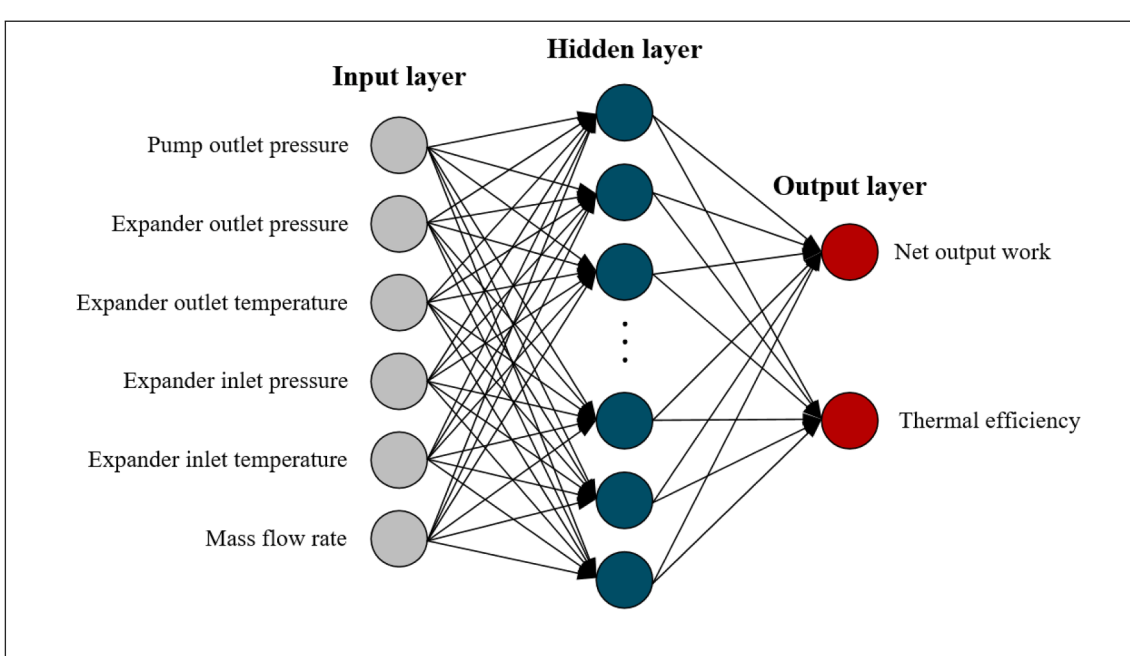


Fig. 3. The model of a BP-ORC neural network with a single hidden layer.

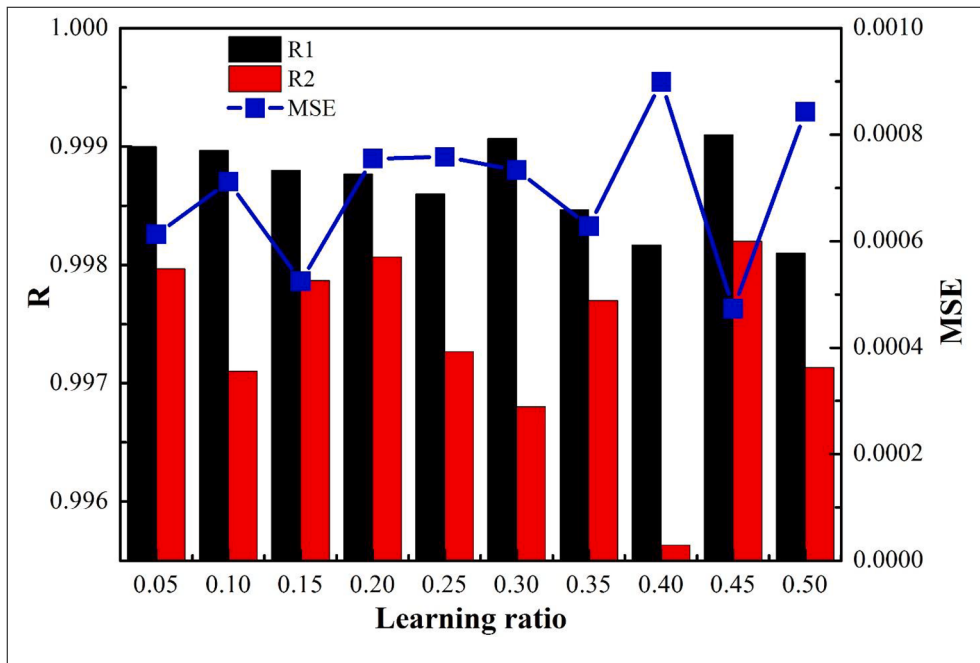


Fig. 4. The effect of different learning rates on the accuracy of this model.

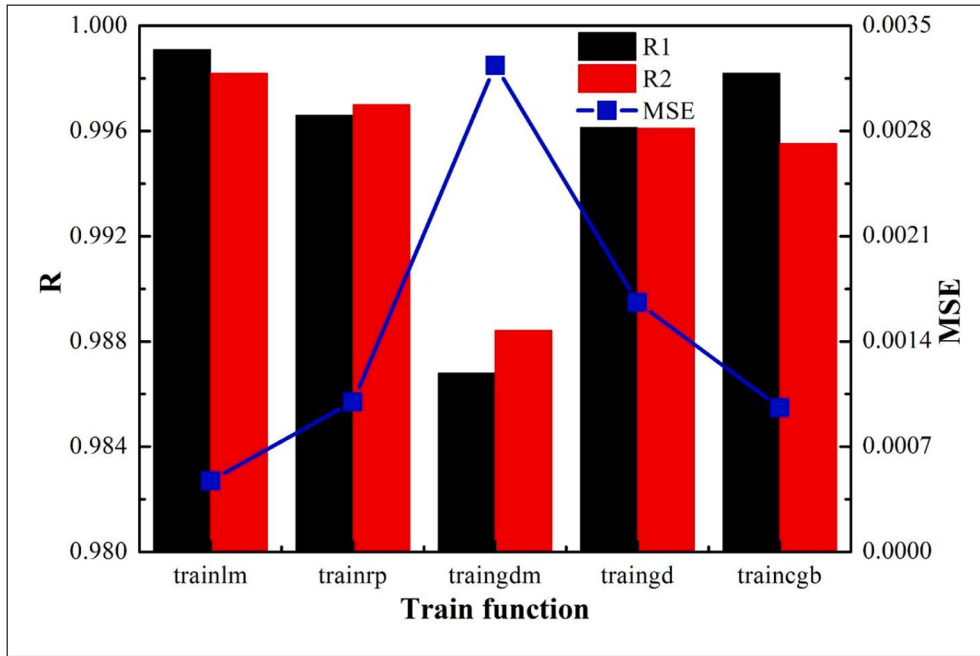


Fig. 5. The effect of the training functions on the accuracy of the model.

minimum MSE of 0.000473 is obtained, while R1 and R2 are 0.991 and 0.9982, respectively. The worst accuracy of the model is yielded by traingdm.

Fig. 6 illustrates the variation of model accuracy with a hidden layer neural number. The hidden layer neural number greatly influence the accuracy of model prediction. A smaller hidden layer neural number will cause the network to fail to learn well and the training accuracy will be affected. A larger hidden layer neural number will lead to an increase in training time and the network is prone to overfitting. Based on the existing empirical formula, the hidden layer neural number is set to change from 2 to 12. From Fig. 6, the MSE and R of this model have no uniform law with the variation of the hidden layer neural number. When

the hidden layer neural number is 7, the minimum MSE of 0.000329 is obtained, with the corresponding respective maximum R for two outputs of 0.9992 and 0.9994.

Based on the above discussion, the learning rate of 0.45, the training function of trainlm, and the hidden layer neural number of 7 are selected to train the neural network model. The specific parameter settings are shown in Table 6, and the operation is shown in Fig. 7.

4.2. Accuracy evaluation for BP-ORC neural network model

4.2.1. Accuracy evaluation of model training

To ascertain the accuracy of the BP-ORC neural network model, 950

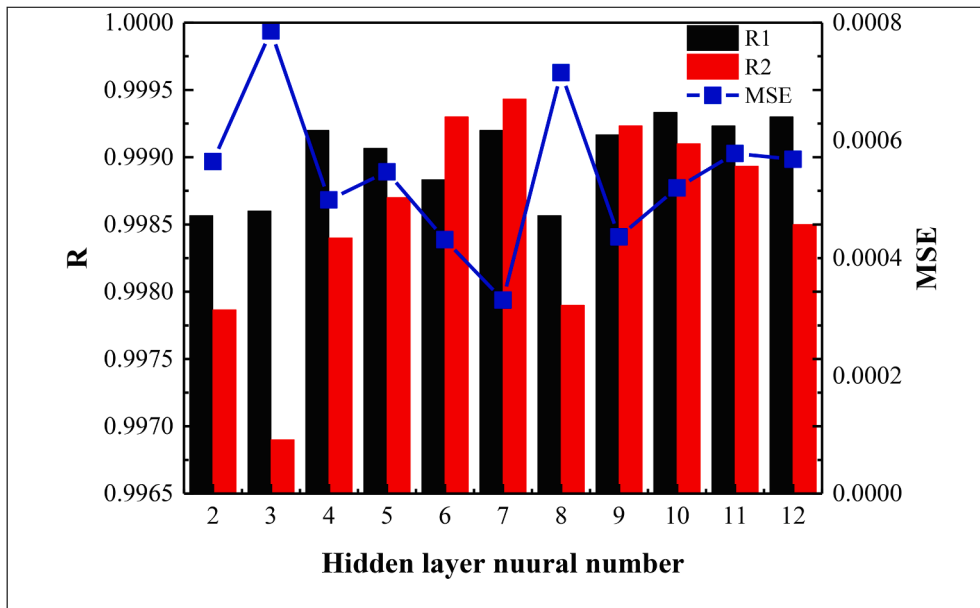


Fig. 6. The effect of the hidden layer neural number on the accuracy of the model.

Table 6
The specific parameter settings.

| Parameter | Value |
|-----------------------|---------|
| Learning rate | 0.45 |
| Neural number | 7 |
| Training function | Trainlm |
| Hidden layer function | Tansig |
| Output layer function | Purelin |

sets of experimental data listed in Table 5 are divided into two parts: the first 800 sets are training samples, and the last 150 sets are test samples. Fig. 8 demonstrates the absolute errors and relative errors of the thermal efficiency obtained by BP-ORC neural network model. The absolute errors of thermal efficiency are between -8×10^{-4} to 8×10^{-4} , and the relative errors are between -1.5% and 1.5%.

Fig. 9 shows the absolute errors and relative errors of the system net output work obtained by the model training and experiment. The absolute errors of net output work are between -0.05 and 0.05 kW and the relative errors of net output work are mostly between -2% and -1%. Only a few data exceed this range, but the maximum is also between -5% and 4%. Based on the above training results, the two output errors are relatively small and the model meets the accuracy requirements.

4.2.2. Accuracy evaluation of model prediction

Furthermore, the accuracy of the model is evaluated at a higher level through the prediction errors of the last 150 data sets. Fig. 10 displays the correlation results of the thermal efficiency predicted by the model. Fig. 10(a) compares the predicted value by the model with the experimental value of the thermal efficiency. The blue line represents experimental data and the red line denotes predicted data. As shown in Fig. 10 (a), the coincidence of the two lines is very well, with only a slight deviation at the inflection points. Fig. 10(b) and (c) show the absolute errors and relative errors of the thermal efficiency. From Fig. 10, the absolute errors of thermal efficiency are between -10×10^{-4} and 6×10^{-4} , and the relative errors are between -1.5% and 1.5%.

Fig. 11 represents the correlation results of net output work predicted by the model. Fig. 11(a) is a comparison of the predicted and the experimental net output work. The matching degree of the two lines is very good, and there is no obvious deviation even at the inflection points, which means that the predicted value is sufficiently close to the

experimental value. Fig. 11(b) and (c) show the absolute errors and relative errors of net output work respectively, with the absolute value of the absolute errors reaching 0.04 kW and the absolute value of the relative errors reaching 3.5%. According to Figs. 10 and 11, the prediction accuracy of this model is very high, and the errors are within an acceptable range.

4.3. Parameter analysis based on BP-ORC model

In this section, the prediction function of the BP-ORC model is utilized to analyze the impact of various operating parameters on the system's overall performance. The operating parameters include pump outlet pressure, mass flow rate, expander inlet temperature and pressure, and expander outlet temperature and pressure. Fig. 12 plots the variation of the system's overall performance with mass flow rate and pump outlet pressure. The pressure and temperature at the expander inlet and outlet are fixed at 6.97 bar, 87 °C, 1.99 bar, and 60 °C, respectively. As shown in Fig. 12(a), the thermal efficiency presents an increasing trend with the mass flow rate, but a parabolic trend with the pump outlet pressure. The thermal efficiency is determined by the net power output and heat input. The rise in mass flow rate causes an increase in net output work, resulting in the increase in thermal efficiency. When the pump outlet pressure goes up, the pump shaft work keeps increasing, while the expander shaft work and heat input increase. The increasing net output work is obvious than the increasing heat input, resulting in the rise in thermal efficiency. However, with a further increase in pump outlet pressure, the increasing heat input has a leading position, and thus the thermal efficiency goes down. Therefore, it exists an optimal matching value between the mass flow rate and the pump outlet pressure. Therefore, the thermal efficiency can be optimized by adjusting these two parameters simultaneously during the experiment.

Fig. 12(b) shows the effect of mass flow rate and pump outlet pressure on the net output work. It can be seen that the net output work presents a smooth increase with pump outlet pressure, but a sharp increase with mass flow rate. The reason for that is the mass flow rate has a significant influence on shaft work, because the shaft work is the product of mass flow rate and enthalpy difference. However, increasing pump outlet pressure ensures a slight increase in enthalpy difference of expander.

The variation of system's overall performance with the expander inlet temperature and pressure are plotted in Fig. 13. The pump outlet

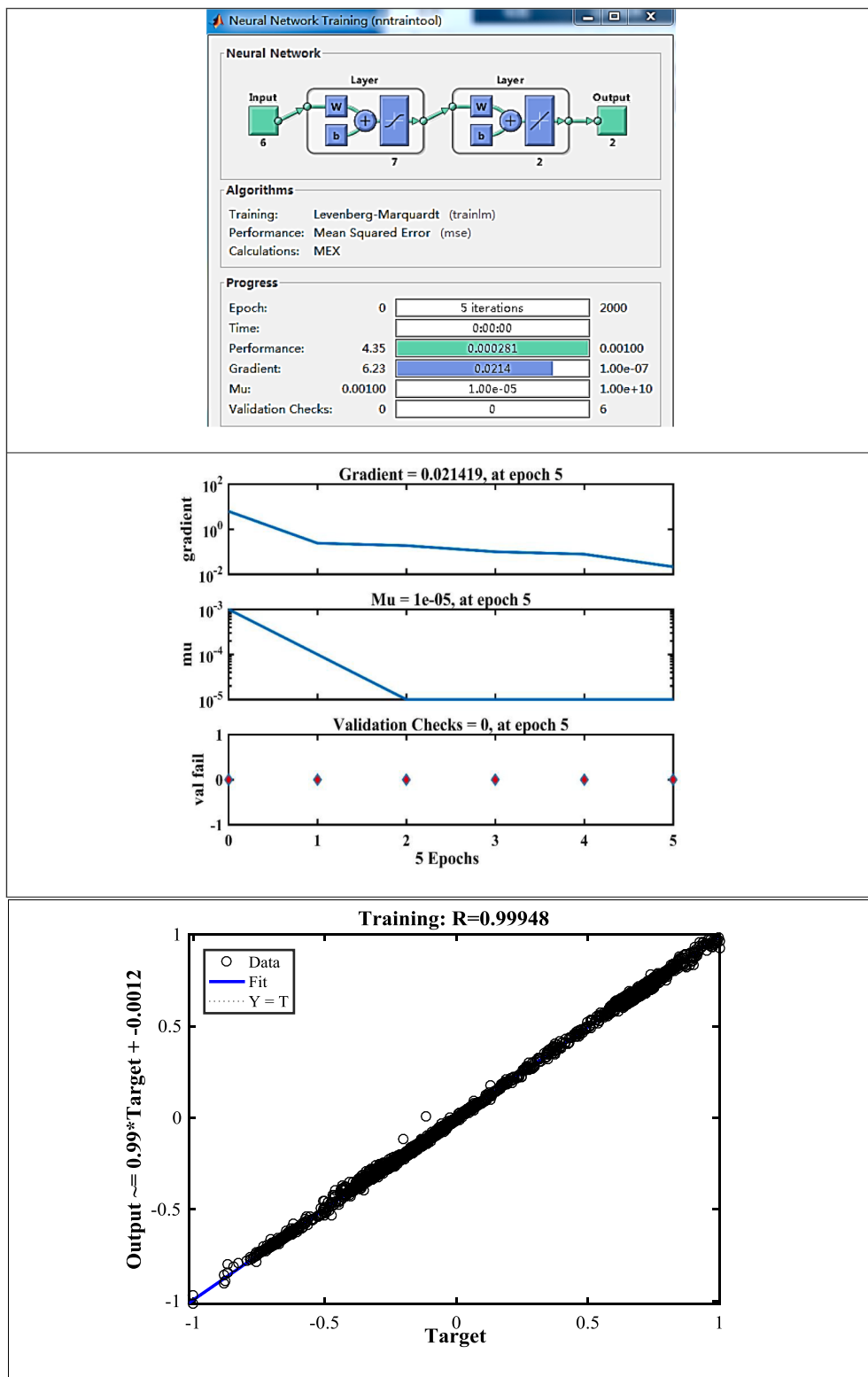


Fig. 7. The operation of the model.

pressure, the expander outlet temperature and pressure, and the mass flow rate are fixed at 7.3 bar, 60 °C, 1.99 bar, and 0.23 kg/s, respectively. The expander inlet temperature increases from 80 to 90°C, and the inlet pressure increases from 5.4 to 6.9 bar. From Fig. 13(a), the expander inlet temperature greatly affects the thermal efficiency. With the increase in expander inlet temperature, the thermal efficiency increases significantly. However, the expander inlet pressure has a slight

fluctuation effect on thermal efficiency. Therefore, the system's thermal efficiency can be enhanced by adjusting the inlet temperature of the expander.

Fig. 13(b) plots the relationship between the net output work and the expander inlet pressure and temperature. The net output work behaves as a parabolic trend with a maximum value with the expander inlet temperature. When the inlet temperature is greater than 86 °C, the net

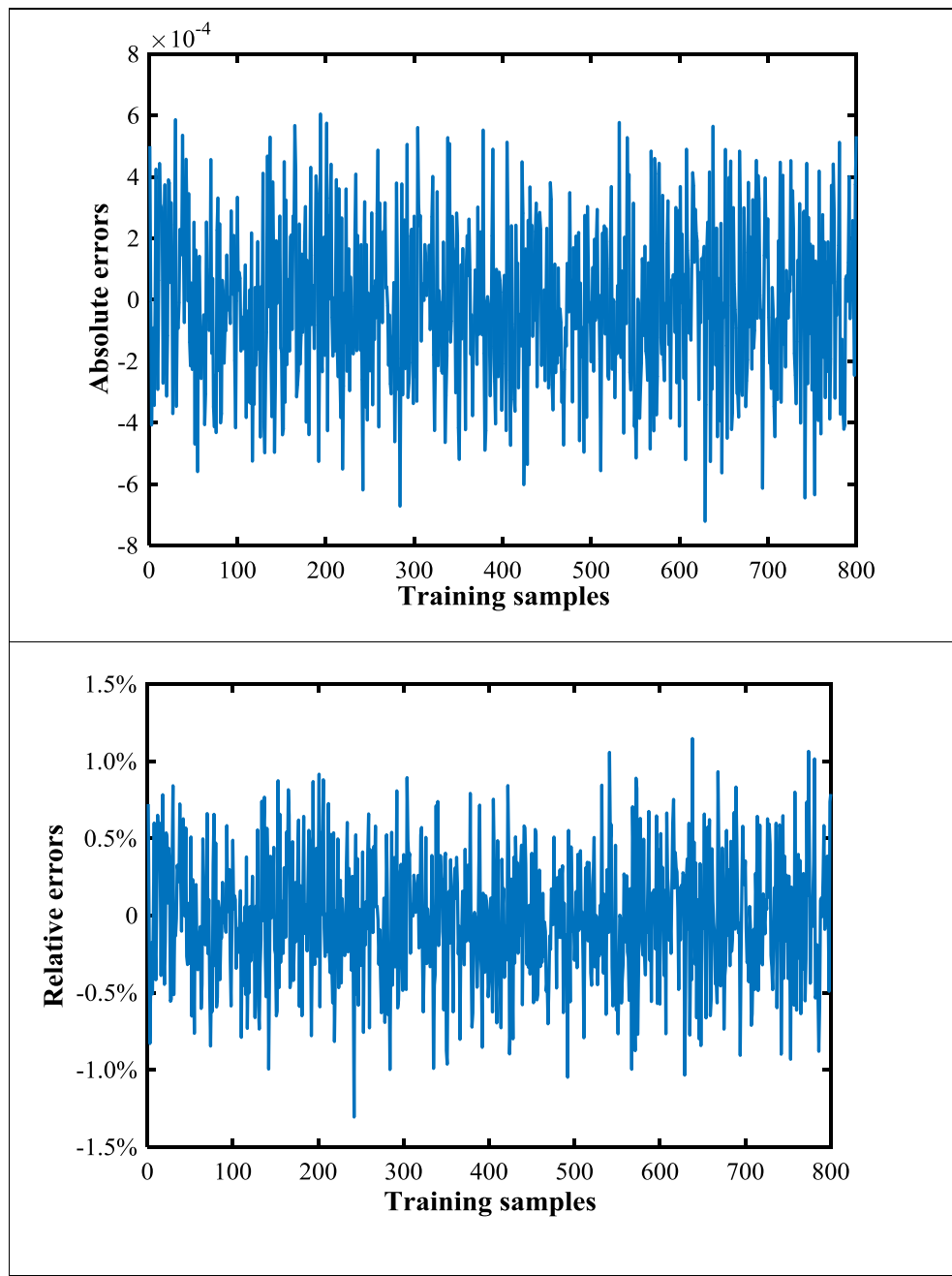


Fig. 8. The absolute errors and relative errors of the thermal efficiency.

output work increases with the expander inlet pressure. The net output work reaches a maximum of 3.25 kW with the expander inlet temperature of 88 °C and pressure of 6.9 bar.

Fig. 14 plots the influence of temperature and pressure at expander outlet on the thermal efficiency and net output work. The pump outlet pressure, the expander inlet temperature and pressure, and the mass flow rate are 7.3 bar, 87 °C, 6.97 bar, and 0.23 kg/s, respectively. The expander outlet temperature ranges from 56 to 66 °C and the outlet pressure is in range of 1.5–2 bar. From Fig. 14(a), the thermal efficiency presents a decreasing trend with the expander outlet temperature, but an increasing trend with the expand outlet pressure, which may be different from the theoretical analysis. The reason for this is the other operation parameters are set as constant values. Increasing the expander outlet temperature ensures a decrease in expander enthalpy difference, resulting in the decrease in expander shaft work and net output work, and causes the deterioration of thermal efficiency. The expander outlet

pressure has a significant influence on the expander operation behavior, especially on the expansion ratio and expander isentropic efficiency. Our previously research [29–31] demonstrated that the expander isentropic efficiency presented a slight decrease first and then a sharp increase with mass flow rate, while the expander isentropic was in range of 69.10–85.17%. Increasing the expander outlet pressure enables an increase in expander isentropic efficiency, resulting in the increase in net output work increase. And thus the thermal efficiency presents an increase trend with the expander outlet pressure. Fig. 14(b) plots the relationship between the net output work and the expander outlet temperature and pressure. The net output work increases slowly first and then decreases sharply with the expander outlet temperature. The net output work reaches the maximum when the outlet temperature is 58 °C. The reason for this is that increasing the expander outlet temperature causes the decrease in expander enthalpy difference. Meanwhile, the pump inlet temperature and pressure have a slight increase

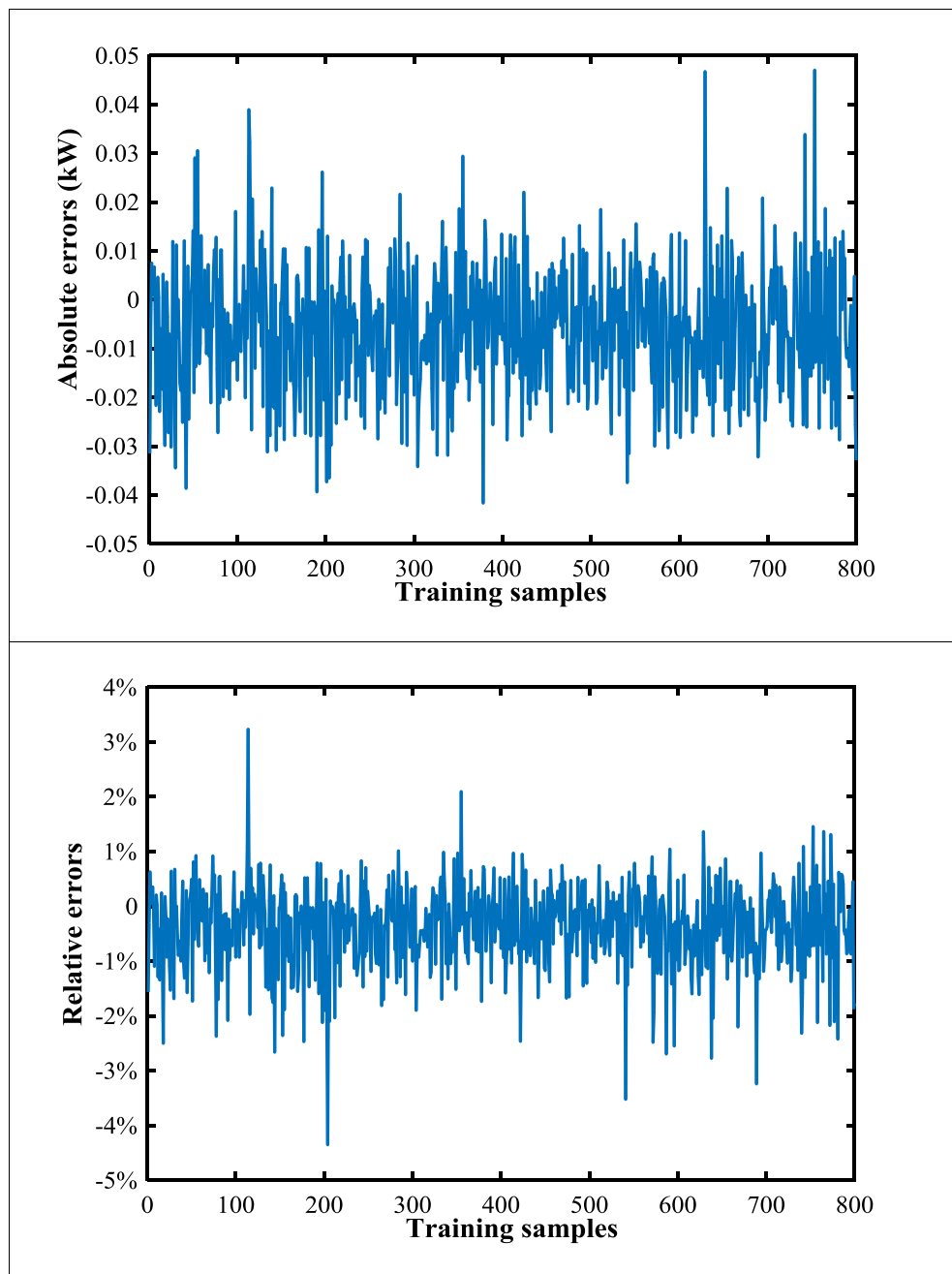


Fig. 9. The absolute errors and relative errors of the system net output work.

with the expander outlet temperature, resulting in the decrease in pump enthalpy difference. The comprehension effect of the decreasing expander enthalpy difference and decreasing pump enthalpy difference causes the parabolic trend in net output work. It can be found that the net output work keeps increasing with the expand outlet pressure, which may be contributed to the sharp variation of the expander isentropic efficiency. In particular, the net output work reaches a maximum of 3.25 kW with the expander outlet temperature of 58 °C and the pressure of 1.8 bar. To sum up, for the purpose of increasing the thermal efficiency during the experiment, priority should be given to increasing the pump outlet pressure, the expander inlet temperature, and reducing the expander outlet temperature. In the same context, improving the net output work should increase the mass flow rate and adjust the appropriate expander inlet and outlet temperature.

4.4. Multi-objective optimization

As demonstrated in Section 4.3, the operation parameters have a significant influence on the system overall performance. The net output work and thermal efficiency are two very important evaluation indexes considered in engineering applications. However, the maximum net power output and maximum thermal efficiency cannot be obtained simultaneously, because they presents different variation with the operation parameters. In order to obtain the optimal system performance and operation parameters, a bi-objective optimization for maximum net output work and maximum thermal efficiency using BP-ORC neural network model is conducted. The operation parameters in Section 4.3 are used as the decision variables, while the net output work and thermal efficiency are selected as the objective functions. The ranges for the six operation parameters are listed in Table 7. Based on the energy balance, the following constraints should be satisfied.

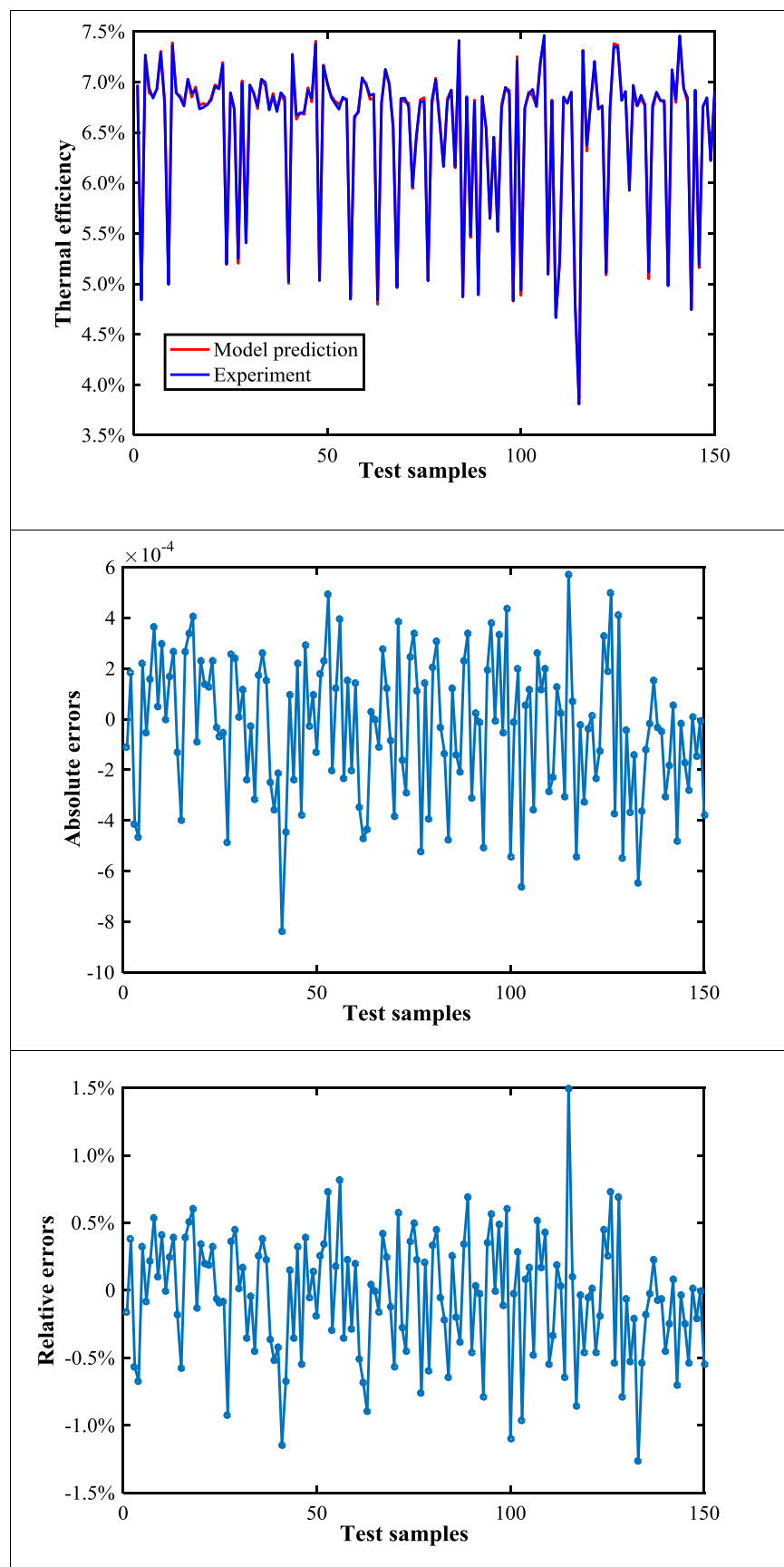


Fig. 10. The correlation results of the thermal efficiency predicted by the model for the test samples.

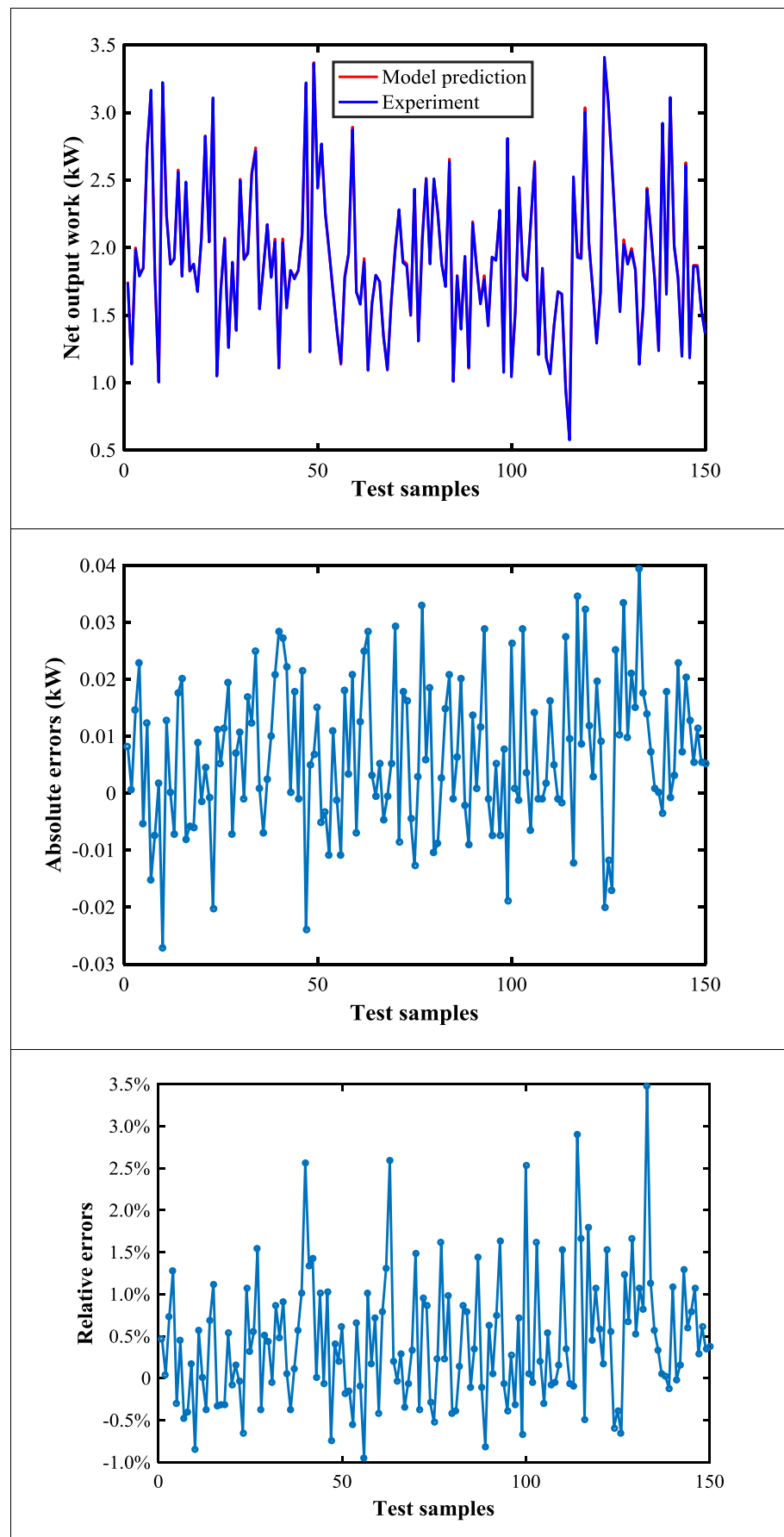


Fig. 11. The correlation results of the net output work predicted by the model for the test samples.

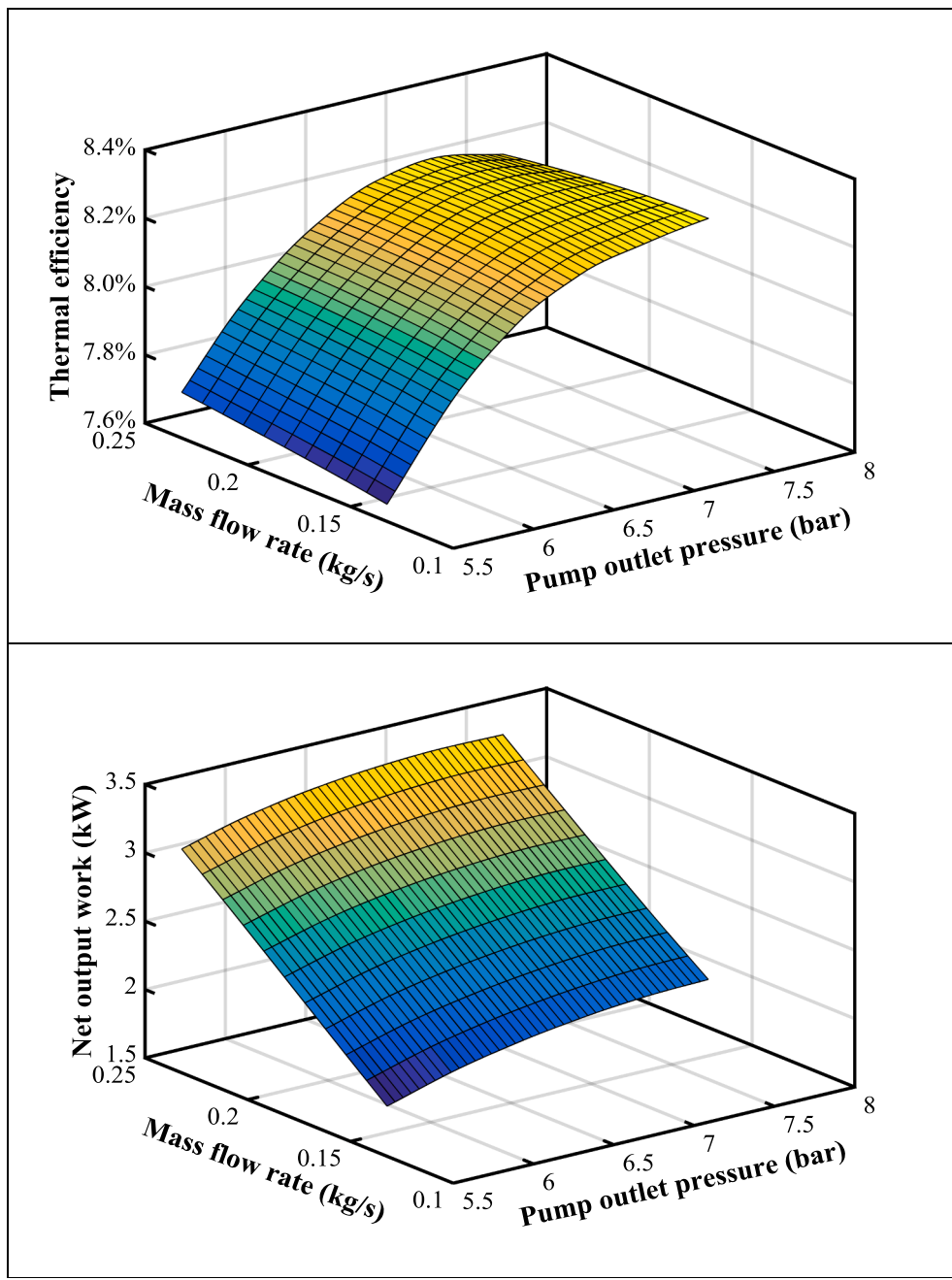


Fig. 12. The variation of the two output parameters with the mass flow rate and pump outlet pressure.

$$P_{in,pump} < P_{out,pump}, T_{in,pump} < T_{out,pump}, P_{out,exp} < P_{in,exp}, T_{out,exp} < T_{in,exp} \quad (11)$$

NSGA-II (Nondominated sorting genetic algorithm-II) is used to conduct the bi-objective optimization. The detailed genetic algorithm parameters are specified according to the following values: population size 70, generation size 70, crossover fraction 0.8 and migration fraction 0.2. The Pareto optimal frontier for maximum net output work and maximum thermal efficiency is obtained and plotted in Fig. 15. It can be found that a tradeoff relationship is appeared between net output work and thermal efficiency. It should be noted that all the optimum design points in the Pareto optimal frontier are non-dominated and could be chosen by the decision makers as optimum operation parameters. Increasing thermal efficiency will inevitably worsen net output work. The maximum thermal efficiency, which exists at point C, is 7.80% with the worst net output work of 1.93 kW, while the maxim net output work of 3.24 kW is obtained at point A with the lowest thermal efficiency of

7.64%. The ideal point does not exist to maximum thermal efficiency and maximum net output work simultaneously. What should be emphasized that the point C is regarded as the single-objective optimization using maximum thermal efficiency as objective function, while the point A is regarded as the single-objective optimization using maximum net output work as objective function. TOPSIS (Technique for Order Preference by Similarity to Ideal Situation), which attempts to choose alternatives that simultaneously have the shortest distance from the positive ideal solution and the farthest distance from the negative-ideal solution, is used to select the Pareto-optimal solution. The Pareto-optimal solution at point B owns the optimum thermal efficiency of 7.76% and the optimum net output work of 2.31 kW. Meanwhile, the optimum operation parameter are listed in Table 8. From Table 8, a higher pump outlet pressure, a higher expander outlet temperature, a higher expander inlet pressure, a lower expander outlet pressure and a lower inlet temperature ensure a better optimization results.

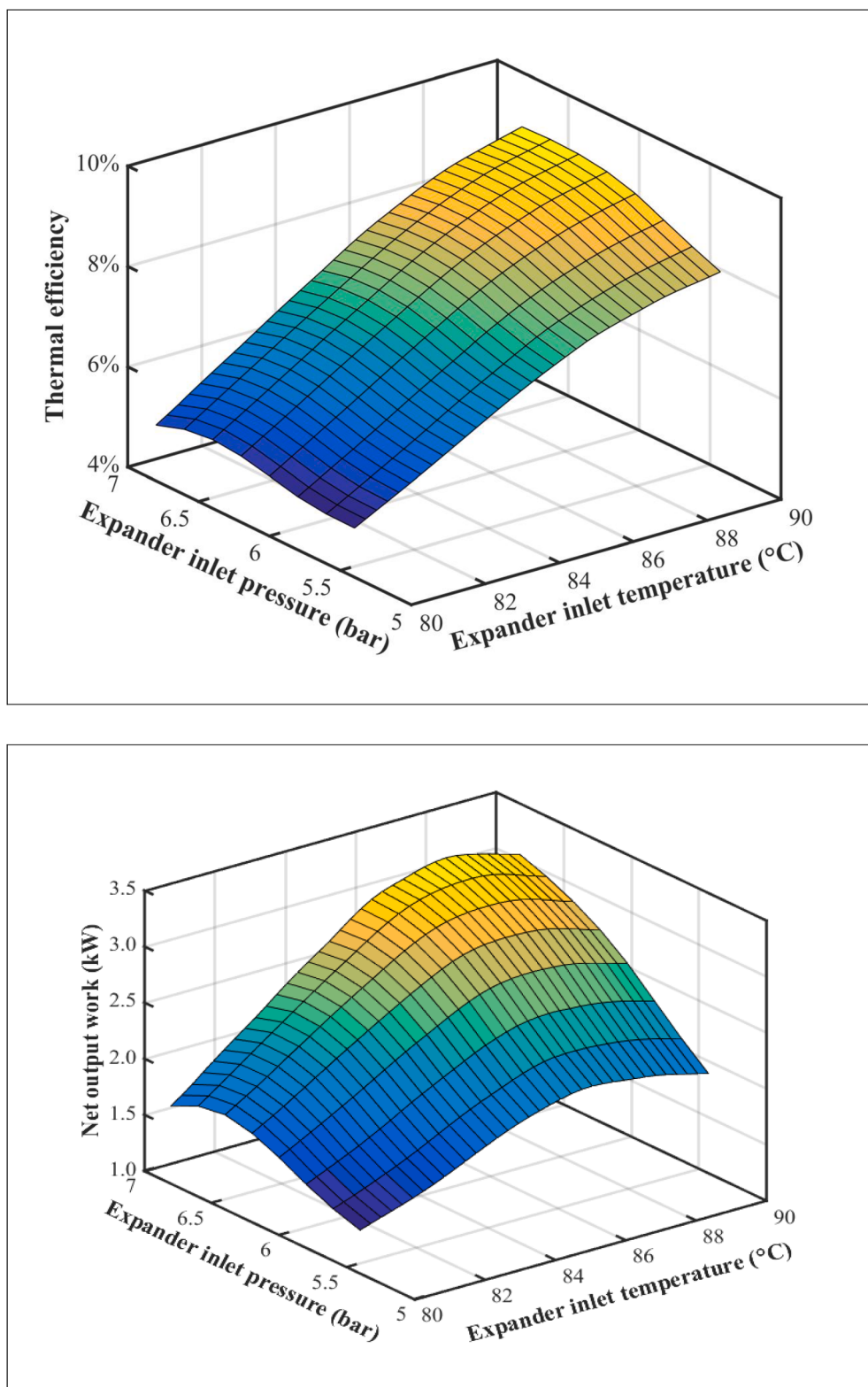


Fig. 13. The variation of the two outputs with inlet temperature and pressure of the expander.

5. Conclusion

Performance prediction and multi-objective optimization for an organic Rankine cycle (ORC) using back propagation (BP) neural network are investigated in this study. A 3 kW ORC experiment platform is used to obtain 950 sets of basic experimental data, and a BP-ORC

model is established based on these experimental data. The prediction accuracy of the BP-ORC model is analyzed according to the errors of the training samples and test samples. The effects of six operation parameters on thermal efficiency and net output work are addressed. In order to make the optimal system, this paper takes the maximum net output work and maximum thermal efficiency as the optimization goals and

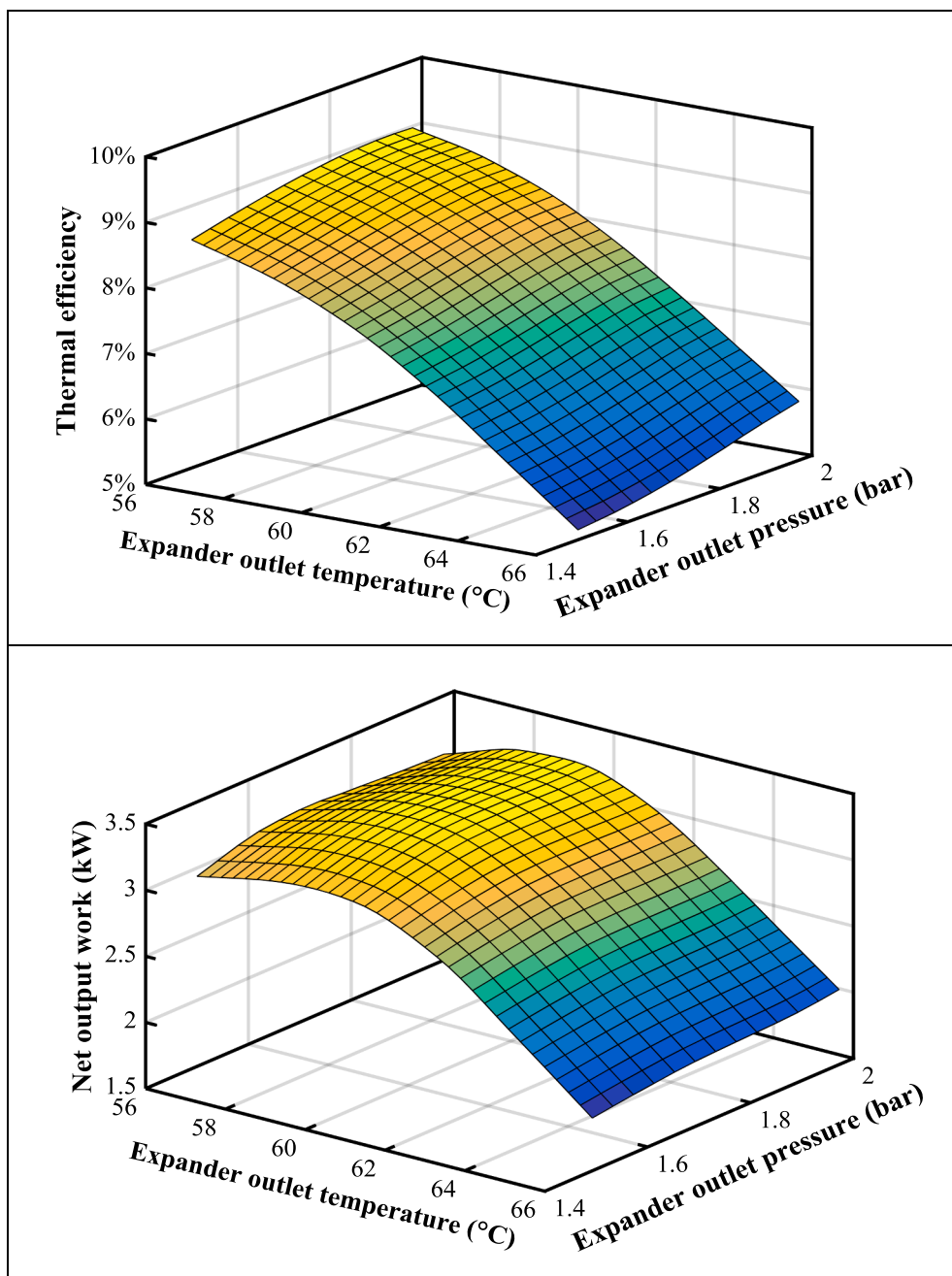


Fig. 14. The effects of expander outlet temperature and outlet pressure on the two outputs.

Table 7
The range of values for the system parameters.

| Optimization variables | Upper | Lower | unit |
|-----------------------------|-------|-------|------|
| Pump outlet pressure | 7.2 | 7.5 | bar |
| Expander outlet temperature | 59 | 61 | °C |
| Expander outlet pressure | 1.7 | 2 | Bar |
| Expander inlet temperature | 88 | 92 | °C |
| Expander inlet pressure | 6.8 | 7.2 | bar |
| Mass fluid rate | 0.14 | 0.24 | kg/s |

optimizes the system parameters at the same time. The results are obtained as follows:

- (1) The parameters of the BP-ORC model based on 950 sets of experimental data are: the learning rate is 0.45, the training

function is trailm, and the hidden layer neural number is 7. The absolute error of the thermal efficiency predicted by the model is in the range of -10×10^{-4} – 6×10^{-4} , and the absolute error of the net output work is -0.03 – 0.04 kW.

- (2) By predicting the effect of various parameters on the system's overall performance, increasing the pump outlet pressure and the expander inlet temperature, or reducing the expander outlet temperature can increase the system's thermal efficiency. Increasing the mass flow rate or matching the expander inlet and outlet temperatures can achieve a higher net output work.
- (3) A tradeoff relation is appeared between net output work and thermal efficiency. Within the range of the above parameters, the maximum thermal efficiency can reach 7.80% and the maximum net output work can reach 3.24 kW. The optimal thermal efficiency and net output work for Pareto-optimal solution is 7.76% and 2.31 kW, respectively.

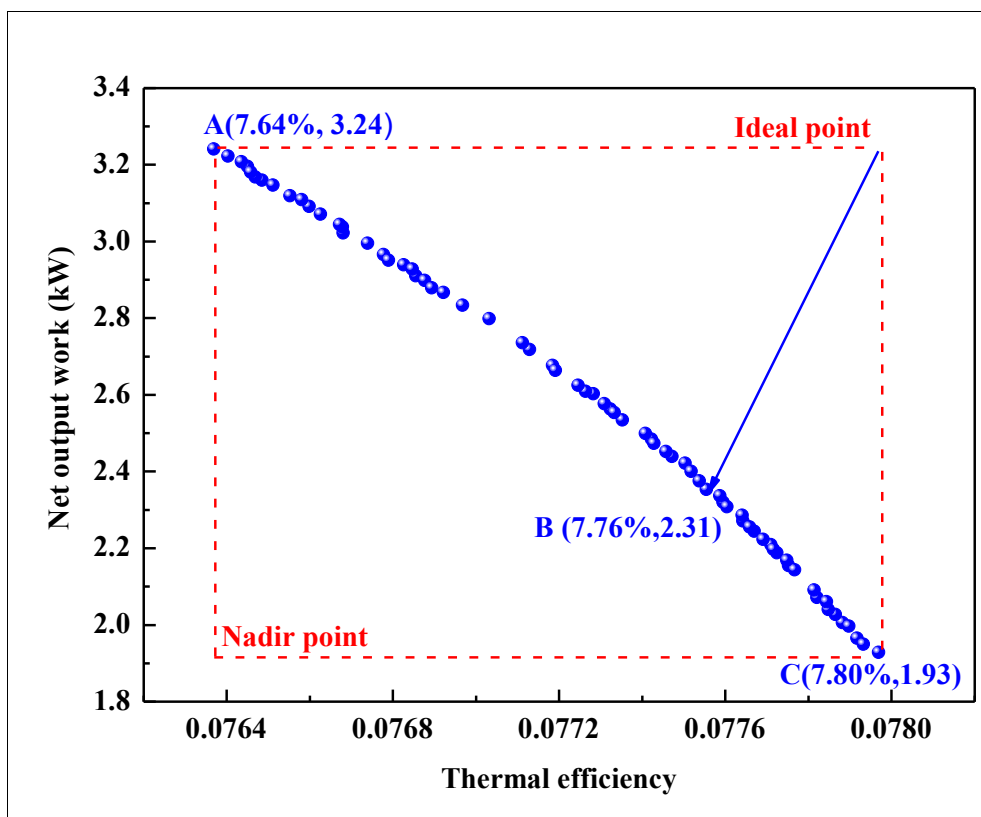


Fig. 15. The Pareto optimal frontier between net output work and thermal efficiency.

Table 8

The parameters corresponding to the optimal value.

| Optimization variables | Value | Unit |
|-----------------------------|-------|------|
| Pump outlet pressure | 7.49 | bar |
| Expander outlet temperature | 61.00 | °C |
| Expander outlet pressure | 1.70 | Bar |
| Expander inlet temperature | 88.00 | °C |
| Expander inlet pressure | 7.20 | bar |
| Mass fluid rate | 0.17 | kg/s |

Credit Author Statement

Yong-qiang Feng and Tzu-Chen Hung conceived of the presented idea. Yu-Zhuang Liu and Xin Wang developed the theory and analyzed the experimental data. Zhi-xia He, Qian Wang and Huan Xi verified the analytical methods. All authors discussed the results and contributed to the final manuscript. All authors have read and agreed to the published version of the manuscript.

Declaration of Competing Interest

The authors declare that they have no known competing financial interests or personal relationships that could have appeared to influence the work reported in this paper.

Acknowledgements

This research work has been supported by the National Natural Science Foundation of China (51806081), the Key Research and Development Program of Jiangsu Province, China (BE2019009-4), the Natural Science Foundation of Jiangsu Province (BK20180882), the Key Research and Development Program of Zhenjiang City, China (SH2019008), the Key Project of Taizhou New Energy Research Institute, Jiangsu University, China (2018-20) and Qinghai Provincial

Natural Science Foundation of China (No. 2018-ZJ-927Q).

References

- [1] Zhou NJ, Wang XY, Chen Z, et al. Experimental study on Organic Rankine Cycle for waste heat recovery from low-temperature flue gas. *Energy* 2013;55:216–25.
- [2] Yamada N, Tominaga Y, Yoshiha T. Demonstration of 10-Wp micro organic Rankine cycle generator for low-grade heat recovery. *Energy* 2014;78:806–13.
- [3] Tian H, Shu GQ, Wei HQ, et al. Fluids and parameters optimization for the organic Rankine cycles (ORCs) used in exhaust heat recovery of Internal Combustion Engine (ICE). *Energy* 2012;47(1):125–36.
- [4] Tian H, Liu LN, Shu GQ, et al. Theoretical research on working fluid selection for a high-temperature regenerative transcritical dual-loop engine organic Rankine cycle. *Energy Convers Manage* 2014;86:764–73.
- [5] Tian H, Chang LW, Gao YY, et al. Thermo-economic analysis of zeotropic mixtures based on siloxanes for engine waste heat recovery using a dual-loop organic Rankine cycle (DORC). *Energy Convers Manage* 2017;136:11–26.
- [6] Song J, Gu CW. Performance analysis of a dual-loop organic Rankine cycle (ORC) system with wet steam expansion for engine waste heat recovery. *Appl Energy* 2015;156:280–9.
- [7] Shu GQ, Wang X, Tian H. Theoretical analysis and comparison of rankine cycle and different organic rankine cycles as waste heat recovery system for a large gaseous fuel internal combustion engine. *Appl Therm Eng* 2016;108:525–37.
- [8] Dong BS, Xu GQ, Li TT, et al. Parametric analysis of organic Rankine cycle based on a radial turbine for low-grade waste heat recovery. *Appl Therm Eng* 2017;126: 470–9.
- [9] Wang DB, Ma YZ, Tian R, et al. Thermodynamic evaluation of an ORC system with a Low Pressure Saturated Steam heat source. *Energy* 2018;149:375–85.
- [10] Uusitalo A, Honkatukia J, Turunen-Saaresti T, et al. A thermodynamic analysis of waste heat recovery from reciprocating engine power plants by means of Organic Rankine Cycles. *Appl Therm Eng* 2014;70(1):33–41.
- [11] Javanshir A, Sarunac N. Thermodynamic analysis of a simple Organic Rankine Cycle. *Energy* 2017;118:85–96.
- [12] Jang Y, Lee J. Comprehensive assessment of the impact of operating parameters on sub 1-kW compact ORC performance. *Energy Convers Manage* 2019;182:369–82.
- [13] Lin CH, Hsu PP, He YL, et al. Investigations on experimental performance and system behavior of 10 kW organic Rankine cycle using scroll-type expander for low-grade heat source. *Energy* 2019;177:94–105.
- [14] Liu C, Wang SK, Zhang C, et al. Experimental study of micro-scale organic Rankine cycle system based on scroll expander. *Energy* 2019;188:115930.
- [15] Sun HC, Qin J, Hung TC, et al. Effect of flow losses in heat exchangers on the performance of organic Rankine cycle. *Energy* 2019;172:391–400.

- [16] Sun HC, Qin J, Yan PG, et al. Performance evaluation of a partially admitted axial turbine using R245fa, R123 and their mixtures as working fluid for small-scale organic Rankine cycle. *Energy Convers Manage* 2018;171:925–35.
- [17] Feng YQ, Hung ZQ, He YL, et al. Operation characteristic and performance comparison of organic Rankine cycle (ORC) for low-grade waste heat using R245fa, R123 and their mixtures. *Energy Convers Manage* 2017;144:153–63.
- [18] Feng YQ, Hung ZQ, Wu SL, et al. Operation characteristic of a R123-based organic Rankine cycle depending on working fluid mass flow rates and heat source temperatures. *Energy Convers Manage* 2017;131:55–68.
- [19] Feng YQ, Hung ZQ, Su TY, et al. Experimental investigation of a R245fa-based organic Rankine cycle adapting two operation strategies: Stand alone and grid connect. *Energy* 2017;141:1239–53.
- [20] Wang TT, Liu LC, Zhu T, et al. Experimental investigation of a small-scale Organic Rankine Cycle under off design conditions: From the perspective of data fluctuation. *Energy Convers Manage* 2019;198:111826.
- [21] Liu LC, Zhu T, Wang TT, et al. Experimental investigation on the effect of working fluid charge in a small-scale Organic Rankine Cycle under off-design conditions. *Energy* 2019;174:664–77.
- [22] Yang FB, Cho H, Zhang H, et al. Artificial neural network (ANN) based prediction and optimization of an organic Rankine cycle (ORC) for diesel engine waste heat recovery. *Energy Convers Manage* 2018;164:15–26.
- [23] Arslan O, Yetik O. ANN based optimization of supercritical ORC-Binary geothermal power plant: Simav case study. *Appl Therm Eng* 2011;31(17–18):3922–8.
- [24] Luo X, Wang Y, Liang J, et al. Improved correlations for working fluid properties prediction and their application in performance evaluation of sub-critical Organic Rankine Cycle. *Energy* 2019;174:122–37.
- [25] Palagi L, Sciubba E, Tocci L. A neural network approach to the combined multi-objective optimization of the thermodynamic cycle and the radial inflow turbine for Organic Rankine cycle applications. *Appl Energy* 2019;237:210–26.
- [26] Emadi MA, Mahmoudimehr J. Modeling and thermo-economic optimization of a new multi-generation system with geothermal heat source and LNG heat sink. *Energy Convers Manage* 2019;189:153–66.
- [27] Rashidi MM, Galanis N, Nazari F, et al. Parametric analysis and optimization of regenerative Clausius and organic Rankine cycles with two feedwater heaters using artificial bees colony and artificial neural network. *Energy* 2011;36(9):5728–40.
- [28] Ziviani D, James NA, Accorsi FA, et al. Experimental and numerical analyses of a 5 kW oil-free open-drive scroll expander for small-scale organic Rankine cycle (ORC) applications. *Appl Energy* 2018;230:1140–56.
- [29] Yang SC, Hung TC, Feng YQ, et al. Experimental investigation on a 3 kW organic Rankine cycle for low-grade waste heat under different operation parameters. *Appl Therm Eng* 2017;113:756–64.
- [30] Feng Y, Hung TC, He YL, et al. Experimental investigation of lubricant oil on a 3 kW organic Rankine cycle (ORC) using R123. *Energy Convers Manage* 2019;182:340–50.
- [31] Pang KC, Chen SC, Hung TC, et al. Experimental study on organic Rankine cycle utilizing R245fa, R123 and their mixtures to investigate the maximum power generation from low-grade heat. *Energy* 2017;133:636–51.
- [32] Feng YQ, Zhang W, Niaz H, He ZX, Wang S, Wang X, et al. Parametric analysis and thermo-economical optimization of a Supercritical-Subcritical organic Rankine cycle for waste heat utilization. *Energy Convers Manage* 2020;212:112773.
- [33] Wu DQ, Zhang DW, Liu SP, et al. Prediction of polycarbonate degradation in natural atmospheric environment of China based on BP-ANN model with screened environmental factors. *Chem Eng J* 2020;125878.